Biochimica et Biophysica Acta 1837 (2014) 1514–1521

Contents lists available at ScienceDirect

Biochimica et Biophysica Acta

journal homepage: www.elsevier.com/locate/bbabio

Excitation relaxation dynamics and energy transfer in fucoxanthin–chlorophyll *a*/*c*-protein complexes, probed by time-resolved fluorescence ☆

Seiji Akimoto [a,b,c,*], Ayaka Teshigahara [b], Makio Yokono [a,c], Mamoru Mimuro [d], Ryo Nagao [e], Tatsuya Tomo [f,g]

[a] Molecular Photoscience Research Center, Kobe University, Kobe 657-8501, Japan
[b] Graduate School of Science, Kobe University, Kobe 657-8501, Japan
[c] CREST, Japan Science and Technology Agency (JST), Kobe 657-8501, Japan
[d] Graduate School of Human and Environmental Studies, Kyoto University, Kyoto 606-8501, Japan
[e] Division of Material Science, Graduate School of Science, Nagoya University, Furo-cho, Chikusa-ku, Nagoya 464-8602, Japan
[f] Faculty of Science, Tokyo University of Science, Tokyo 162-8601 Japan
[g] PRESTO, Japan Science and Technology Agency (JST), Saitama 332-0012, Japan

ARTICLE INFO

Article history:
Received 24 September 2013
Received in revised form 1 February 2014
Accepted 4 February 2014
Available online 12 February 2014

Keywords:
Fucoxanthin–chlorophyll *a*/*c* protein
Light harvesting
Photosynthesis
Energy transfer
Time-resolved spectroscopy

ABSTRACT

In algae, light-harvesting complexes contain specific chlorophylls (Chls) and keto-carotenoids; Chl *a*, Chl *c*, and fucoxanthin (Fx) in diatoms and brown algae; Chl *a*, Chl *c*, and peridinin in photosynthetic dinoflagellates; and Chl *a*, Chl *b*, and siphonaxanthin in green algae. The Fx–Chl *a*/*c*-protein (FCP) complex from the diatom *Chaetoceros gracilis* contains Chl c_1, Chl c_2, and the keto-carotenoid, Fx, as antenna pigments, in addition to Chl *a*. In the present study, we investigated energy transfer in the FCP complex associated with photosystem II (FCPII) of *C. gracilis*. For these investigations, we analyzed time-resolved fluorescence spectra, fluorescence rise and decay curves, and time-resolved fluorescence anisotropy data. Chl *a* exhibited different energy forms with fluorescence peaks ranging from 677 nm to 688 nm. Fx transferred excitation energy to lower-energy Chl *a* with a time constant of 300 fs. Chl *c* transferred excitation energy to Chl *a* with time constants of 500–600 fs (intra-complex transfer), 600–700 fs (intra-complex transfer), and 4–6 ps (inter-complex transfer). The latter process made a greater contribution to total Chl *c*-to-Chl *a* transfer in intact cells of *C. gracilis* than in the isolated FCPII complexes. The lower-energy Chl *a* received excitation energy from Fx and transferred the energy to higher-energy Chl *a*. This article is part of a Special Issue entitled: Photosynthesis Research for Sustainability: Keys to Produce Clean Energy.

1. Introduction

Light-harvesting antenna complexes exist as integral membrane antenna complexes or peripheral membrane antenna complexes. These complexes absorb light energy and transfer it to reaction centers as excitation energy. In contrast to the reaction center complexes, light-harvesting complexes (LHCs) are remarkably diverse in their pigment contents [1]; for example, LHCs of higher plants and green algae contain chlorophyll (Chl) *b* and Chl *a*, whereas those of diatoms, brown algae and photosynthetic dinoflagellates contain Chl *c*, in addition to Chl *a*. The spectral properties of Chls depend on their conjugation structures; Chl *a* and Chl *b* are chlorin-type pigments with the 17,18-dihydroporphyrin system, whereas Chl *c* is a porphyrin-type pigment with a fully unsaturated porphyrin system. Chl *a* exhibits two strong absorption bands in the violet and red regions, known as the Soret band and the Qy band, respectively. The latter corresponds to the S_1–S_0 transition of Chl. Chl *b* and Chl *c* extend the wavelength regions of light that can be used for photosynthesis. Compared with Chl *a*, Chl *b* absorbs light energy at longer wavelengths in the Soret band and at shorter wavelengths in the Qy band [2]. The Soret band of Chl *c* is located at almost the same wavelength as the Chl *b* Soret band, whereas its S_1–S_0 transition is at a shorter wavelength [2]. The combination of Chl *a*, Chl *b*, and Chl *c* allows LHCs to utilize light energy in the violet-to-blue region, and the orange-to-red region. The light energy captured by Chl *b* or Chl *c* is transferred to Chl *a* for photosynthesis. In Chl *b*-containing LHCs, such as the *Codium fragile* LHCII and the *Arabidopsis thaliana* LHCII, Chl *b*-to-Chl *a* energy transfer occurs in 700–800 fs, with a high efficiency of almost unity [3,4]. Because of the conjugation structure of Chl *c*, the strength of

Abbreviations: Car, carotenoid; Chl, chlorophyll; FDAS, fluorescence decay-associated spectrum (spectra); Fx, fucoxanthin; LHC, light-harvesting chlorophyll *a*/*b*-binding complex; PS, photosystem; Siph, siphonaxanthin; TRFS, time-resolved fluorescence spectrum (spectra)

☆ This article is part of a Special Issue entitled: Photosynthesis Research for Sustainability: Keys to Produce Clean Energy.

* Corresponding author at: Molecular Photoscience Research Center, Kobe University, Kobe 657-8501, Japan. Fax: +81 78 803 5705.
E-mail address: akimoto@hawk.kobe-u.ac.jp (S. Akimoto).

http://dx.doi.org/10.1016/j.bbabio.2014.02.002
0005-2728/

electronic transition for its S_1–S_0 transition is weaker than that of Chl *b*, which might be a disadvantage for energy transfer to Chl *a* [5].

Besides Chls, LHCs contain specific carotenoids (Cars) [6]. Cars can be classified into two groups based on their conjugation structure; conjugated polyenes [7,8], and keto-Cars, which have a keto-carbonyl group in the conjugated double-bond system [9]. The LHCs of higher plants have the polyene-type Car, lutein, as the major Car [10–12]. In algae, the main Cars in LHCs are the keto-Cars, siphonaxanthin (Siph), peridinin, and fucoxanthin (Fx), which work as efficient antenna pigments harvesting blue-to-green light [9,13–15]. This is ecologically advantageous under the green-light-rich conditions under water. The keto-Cars have a conjugation structure with eight CC double bonds and one CO double bond. The optical properties of keto-Cars strongly depend on the surrounding molecules. The absorption spectrum of Siph showed clear vibrational bands in *n*-hexane, as observed for lutein. In methanol, however, the absorption spectrum of Siph lost its structure and showed enhanced absorbance in the longer wavelength region, which is not the case for lutein. It was expected that Car–protein interactions strongly affect light absorption by keto-Cars in LHCs. Our previous studies on Siph based on time-resolved fluorescence anisotropy analyses confirmed that a new electronic state (S_{kc}) exists between the S_2 state and the S_1 state [14].

Diatoms, which are currently the most successful class of phytoplankton in the world's oceans and freshwater environments [16,17], contain a unique LHC, the Fx–Chl *a*/*c*-protein (FCP) complex. This complex possesses the keto-Car, Fx, and the porphyrin-type Chl, Chl *c*. Several groups have reported the isolation and characterization of FCP complexes from various diatom species [18–24]. We detected three major FCP bands, which were named as FCP-A, FCP-B, and FCP-C, by SDS-PAGE with thylakoid membranes from a marine centric diatom *Chaetoceros gracilis* and isolated the FCP-A-enriched and FCP-B/C-enriched complexes (FCP-A oligomer and FCP-B/C trimer, respectively) by sucrose gradient centrifugation and clear-native PAGE after solubilizing the thylakoids [22]. The association of these isolated FCP complexes with photosystem (PS) II and/or PSI is still unknown. There are very few experimental proofs for PS (especially PSII)-associated FCPs.

We previously reported the isolation of oxygen-evolving PSII particles containing a large amount of FCP, namely PSII–FCPII supercomplex, from the diatom, *C. gracilis* [25]. Using the PSII–FCPII supercomplex, we succeeded in isolating the FCPII complex and analyzed its spectral properties [26]. In the present study, we examined ultrafast energy transfer in the FCPII complex by femtosecond time-resolved fluorescence spectroscopy.

2. Experimental

2.1. Preparation of FCPII

Isolation was performed at 277 K unless otherwise indicated. The marine centric diatom, *C. gracilis* Schütt (UTEX LB 2658), was grown in artificial seawater under continuous low-light conditions (30 μmol photons m^{-2} s^{-1}) according to Nagao et al. [25,27]. The PSII–FCPII supercomplex was isolated by differential centrifugation after solubilizing thylakoids with Triton X-100 according to Nagao et al. [25]. The FCPII complex was prepared as described by Nagao et al. [26]. Briefly, the PSII–FCPII supercomplex was treated with Triton X-100. After centrifugation, the supernatant was subjected to anion-exchange chromatography. The FCPII-enriched fraction was eluted after most of the PSII-enriched fraction had eluted from column, and was then subjected to sucrose centrifugation. The FCPII complex was collected from the upper sucrose layer, immediately frozen in liquid nitrogen, and then stored at 213 K until spectroscopic analysis. The isolated FCPII complex was composed of FCP-A, FCP-B, and FCP-C. The stoichiometry of the FCP bands on SDS-PAGE (FCP-A:FCP-B:FCP-C) was approximately 1:1:1 [26]. Note that the terms FCP-A, FCP-B, or FCP-C refer to a group of FCPs.

2.2. Measurements and analyses

Steady-state absorption and fluorescence spectra were measured with a JASCO V-650 spectrophotometer (JASCO, Tokyo, Japan) and a spectrofluorometer (JASCO FP-6600), respectively, at 278 K. Time-resolved fluorescence spectra (TRFS) and polarized fluorescence were measured by the fluorescence up-conversion method as described previously [28], at 285 K for the FCPII complex and at 293 K for Fx. The excitation wavelength was 425 nm, at which all pigments were simultaneously excited. To observe the time evolution of fluorescence polarization, fluorescence kinetics ($I(t)$) were observed for two polarization components that are orthogonal to each other. After polarization components of the fluorescence signals, which were parallel ($I_{//}(t)$) and perpendicular ($I_{\perp}(t)$) to the excitation laser pulse, were measured alternately, the fluorescence rise and decay curves [$I_F(t)$, isotropic fluorescence kinetics] were calculated as follows:

$$I_F(t) = I_{\parallel}(t) + 2I_{\perp}(t). \tag{1}$$

The fluorescence anisotropy ($r(t)$) was calculated as follows:

$$r(t) = \frac{I_{\parallel}(t) - I_{\perp}(t)}{I_{\parallel}(t) + 2I_{\perp}(t)}. \tag{2}$$

To obtain TRFS, the fluorescence rise and decay curves were obtained by measuring the polarization component of the fluorescence signals at the magic angle to the excitation laser pulse. The fluorescence rise and decay curves were analyzed by global analysis to obtain fluorescence decay-associated spectra (FDAS) [29]. In this analysis, fluorescence rise and decay curves at different wavelengths were fitted by sums of exponentials with common time constants.

$$I_F(\lambda, t) = \sum_{i=1}^{n} A_i(\lambda) \exp\left(-\frac{t}{\tau_i}\right) \tag{3}$$

The amplitudes ($A_i(\lambda)$) gave the FDAS of each time-constant.

3. Results

3.1. Steady-state absorption and fluorescence spectra

The steady-state absorption and fluorescence spectra of the FCPII complex at 278 K are shown in Fig. 1. In the wavelength region related to the lowest excitation states of Chls, Chl *a* showed a prominent absorption peak at 672 nm (Qy(0,0)) with its vibrational band around 645 nm (Qy(1,0)), whereas the red-most absorption peak of Chl *c* was located around 634 nm [30]. In addition, Chl *a* and Chl *c* showed Soret

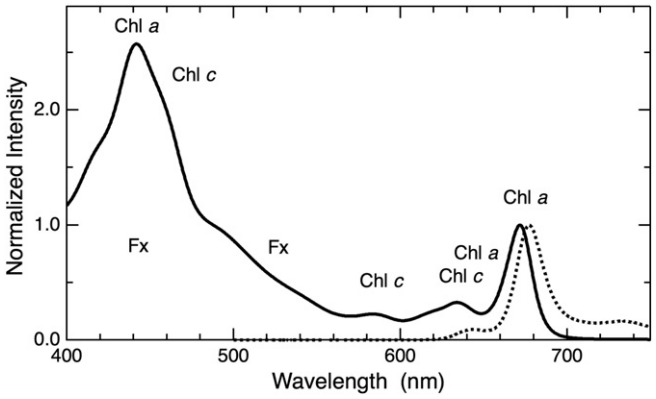

Fig. 1. Steady-state absorption (solid line) and fluorescence (dotted line) spectra of the FCPII complex normalized at Chl *a* Qy band. Excitation wavelength was 425 nm for fluorescence spectrum.

bands at 442 nm and around 460 nm, respectively. The Fx absorption bands were located in the wavelength region shorter than 560 nm, in which two bands were recognized by the second derivative of the absorption spectra at 80 K [26]. The green absorption band is the characteristic band for algal keto-Cars. In the fluorescence spectrum, there was a main peak at 677 nm with a vibrational band around 735 nm, and there was a faint peak at 643 nm. The peak at 677 nm was assigned to Chl *a* fluorescence, whereas that at 643 nm was assigned to Chl *c* fluorescence. Although Chl *a* Qx fluorescence can be observed around 643 nm [31], its contribution to steady-state fluorescence is negligibly small because of its short lifetime. In the fluorescence spectrum of the FCPII complex, there was a clear peak for Chl *c* (Fig. 1). However, this peak was absent in the fluorescence spectrum of the *C. gracilis* cells (Fig. S1). These results indicated that in addition to intra-complex energy transfer, inter-complex energy transfer is significant for Chl *c* in the FCPII complex. There was no apparent peak for Chl *b* in the fluorescence spectra of the *C. fragile* LHCII and the *A. thaliana* LHCII, even the spectra of isolated LHCII [3,14], suggesting that excitation energy harvested by Chl *b* can be efficiently transferred to Chl *a* within the LHCII complex. Fluorescence from Fx was not detected by steady-state measurements.

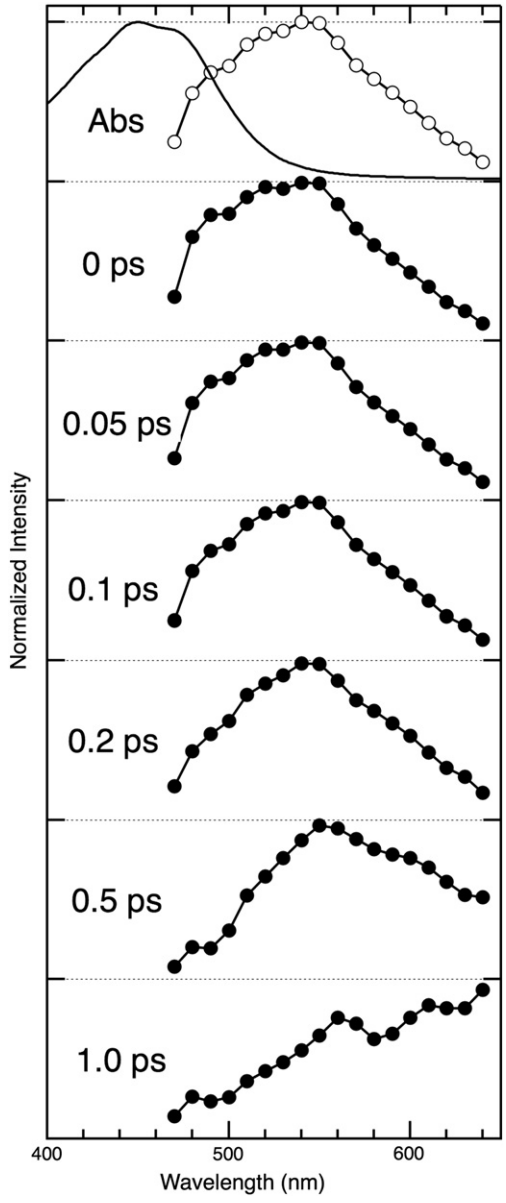

Fig. 2. Normalized time-resolved fluorescence spectra of Fx in solution excited at 425 nm (lines with closed circles). Figure shows absorption spectrum (Abs) and fluorescence spectrum (line with open circles) reconstructed from the first and second shortest-lived components of fluorescence decay-associated spectra shown in Fig. 3.

3.2. Time-resolved fluorescence spectra of fucoxanthin in solution

Fig. 2 shows the TRFS of Fx in ethanol, together with the fluorescence spectrum reconstructed as the sum of the FDAS with the first and second shortest lifetimes shown below (Fig. 3). At the early stage, the spectra represented the mirror image of the absorption spectrum. As the delay time increased, the relative intensities in the longer wavelength region increased. This time-dependent change in spectral shape was analyzed by a global analysis with three lifetime components; 80 fs, 200 fs, and longer than 1 ps (Fig. 3). The behavior of Fx was essentially the same as that observed for Siph in solution [32], although the shortest lifetime was longer for Fx than for Siph. Therefore, we assigned these three FDAS to fluorescences from the S_2 state, the intermediate state between the S_2 and S_1 states (the S_{kc} state), and vibrationally excited states in the S_1 state. This relaxation process might be a common process in keto-Cars with conjugations of eight CC double bonds and one CO double bond [32]. Two lifetimes shorter than 1 ps were also resolved for Fx by a transient absorption measurement [33]. The reconstructed fluorescence spectrum was the mirror image of the absorption spectrum. This is because the contributions of the second (200 fs) and third (>1 ps) FDAS to total fluorescence were smaller than that of the first FDAS (80 fs). The sizes of the contributions are closely related to the strengths of the S_2–S_0, S_{kc}–S_0, and S_1–S_0 transitions, and the lifetimes of their respective excited states.

3.3. Time-resolved fluorescence spectra of the FCPII complex

TRFS of the FCPII complex are shown in Fig. 4, together with a fluorescence spectrum reconstructed as the sum of the first and second FDAS (Fig. 5). At the early stage, the spectra showed three peaks: two sharp bands around 500 nm and 680 nm, and a remarkably broad

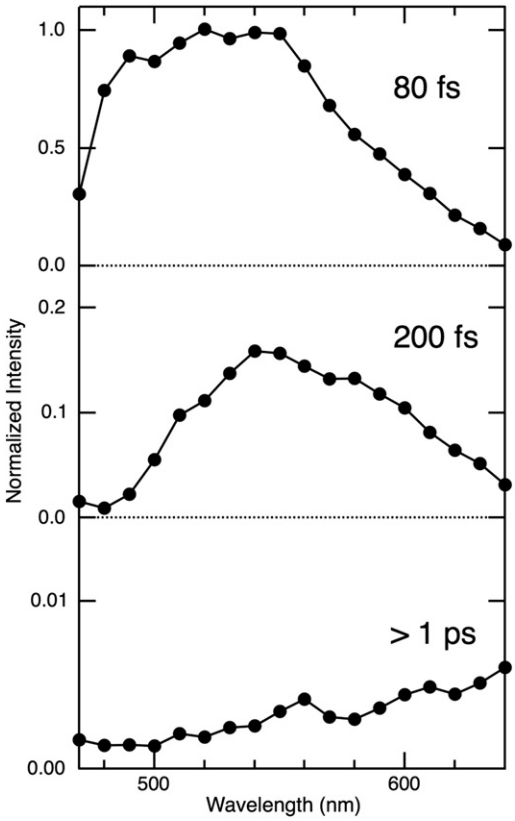

Fig. 3. Fluorescence decay-associated spectra of Fx in solution excited at 425 nm.

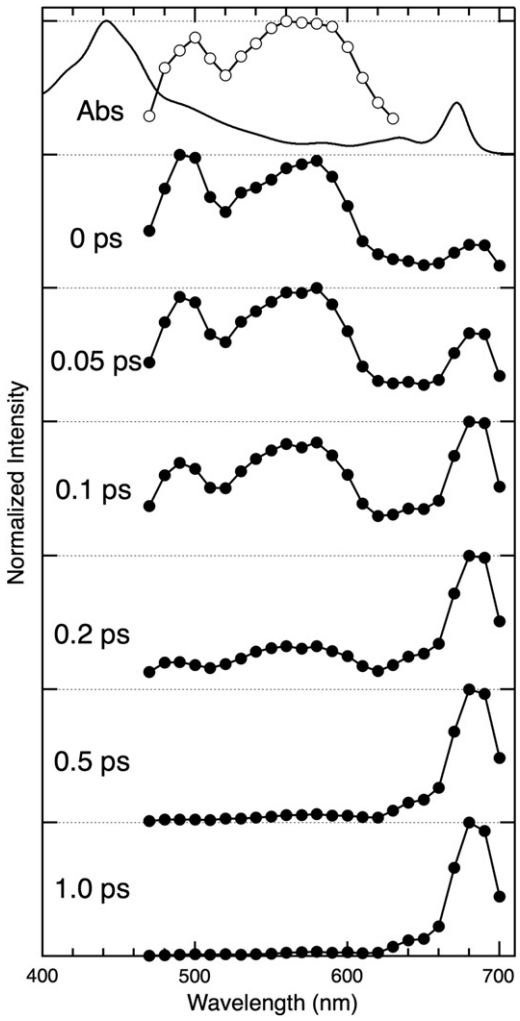

Fig. 4. Normalized time-resolved fluorescence spectra of FCPII complex excited at 425 nm (lines with closed circles). Figure shows absorption spectrum (Abs) and fluorescence spectrum (line with open circles) reconstructed from the first and second shortest-lived components of fluorescence decay-associated spectra shown in Fig. 5.

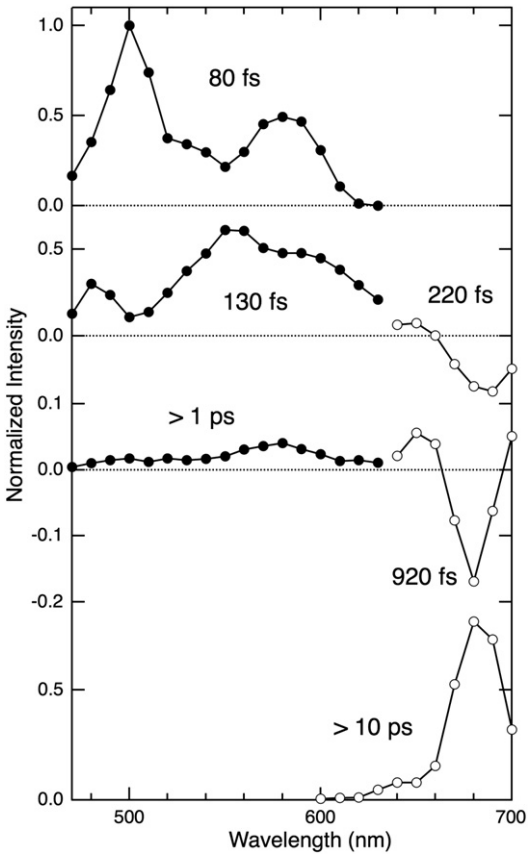

Fig. 5. Fluorescence decay-associated spectra of FCPII complex excited at 425 nm. Time constants required for analysis in the shorter wavelength region (Fx fluorescence and the Chl Soret-band fluorescence regions) (closed circle) differed from those used for analyses in the longer wavelength region (the Chl Q-band fluorescence region) (open circle).

band around 560 nm. As the delay time increased, the relative intensity of the 500-nm band decreased. This was followed by a decrease in the relative intensity of the 560-nm band, and a corresponding increase in the relative intensity of the 680-nm band. These changes were analyzed by a global analysis with three decay components in the shorter wavelength region; 80 fs, 130 fs, and longer than 1 ps, and with three lifetime components in the longer wavelength region; 220 fs, 920 fs, and longer than 10 ps (Fig. 5). In the shorter wavelength region, the 80-fs FDAS showed a sharp band at 500 nm and a broad band around 580 nm. Since the Fx fluorescence band was not sharp (Figs. 2 and 3), it was not reasonable to assign the 500-nm band to Fx fluorescence. Hence, the main contributor to the 500-nm band was likely fluorescence(s) from the Soret band(s) of Chl *a* and/or Chl *c*. In solution, the lifetime of the Chl *a* Soret band was too short to be evaluated, whereas those of Chls c_1 and c_2 were ~50 fs (Fig. 6), suggesting that Chl *c*, rather than Chl *a*, contributed to the 500-nm band. The energy difference between the 500-nm and 580-nm bands was ~2800 cm^{-1}, which is too large to assign the 580-nm band to a vibrational band of Chl *c* Soret fluorescence (the 500-nm band). Therefore, it was more reasonable to assign the 580-nm band to Fx fluorescence. The 80-fs FDAS could be interpreted as a combination of Chl *c* Soret fluorescence and Fx fluorescence. The 130-fs FDAS exhibited a broad band around 550 nm. Chls do not show a fluorescence peak around 550 nm; therefore, the 130-fs FDAS was assigned to Fx fluorescence, although the assignment of the peak at 480 nm was not necessarily clear. In the longer wavelength region, the first (220 fs) and the second (920 fs) FDAS exhibited positive peaks around 640–650 nm and negative peaks around 680–690 nm. As observed in the steady-state fluorescence spectrum, Chl *c* and Chl *a* emitted fluorescence with peaks at 643 nm and 677 nm, respectively. Accordingly, the combinations of the positive and negative peaks with time constants of 220 fs and 920 fs were indicative of Chl *c*-to-Chl *a* energy transfers. However, it should be noted that fluorescence from the Chl *a* Qx band can be detected around 640–650 nm as a short-lived component [31], and that fluorescence kinetics of the Chl *a* Qy band contain a rise component of 120 fs [3]. Therefore, the Qx–Qy internal conversion might have contributed to the 220-fs FDAS. The longest-lived spectral component was the sum of Chl *c* and Chl *a* fluorescences. In the Chl *a* fluorescence region, a peak was located at 690 nm in the 220-fs FDAS, whereas it was slightly shifted to the shorter wavelength in the 920-fs and the longest-lived FDAS. These results suggest that excitation energy was distributed around lower energy Chl *a* at the very beginning and then equilibrated with time. This interpretation is supported by the existence of positive amplitude at 700 nm in the 920-fs FDAS. The relaxation processes analyzed by the global analysis are summarized in Table 1.

3.4. Fluorescence rise and decay curves of the FCPII complex

Global analysis is a very convenient and useful method to examine relaxation dynamics based on spectral properties. However, time constants are mainly determined by components with large amplitudes, and so smaller time-dependent changes can be missed. Therefore, it follows that our descriptions in the previous section represent an "averaged" picture of relaxation dynamics in the FCPII complex. To

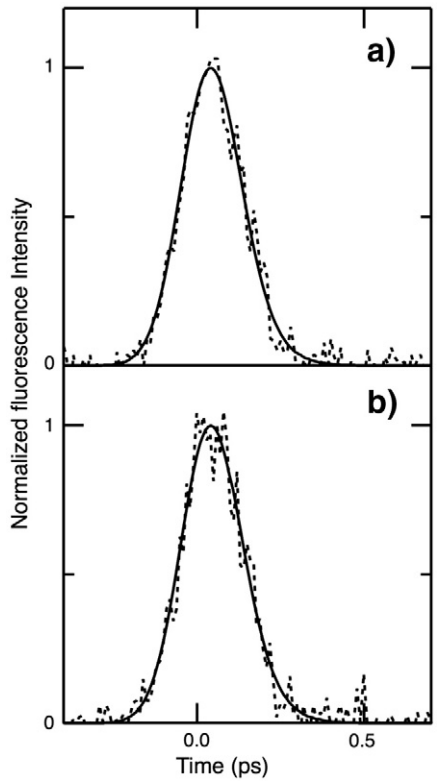

Fig. 6. Fluorescence decay curves of Chl *c* in solution excited at 425 nm: (a) Chl c_1 and (b) Chl c_2. Dotted lines and solid lines show observed fluorescence rise and decay curves and best-fit functions, respectively.

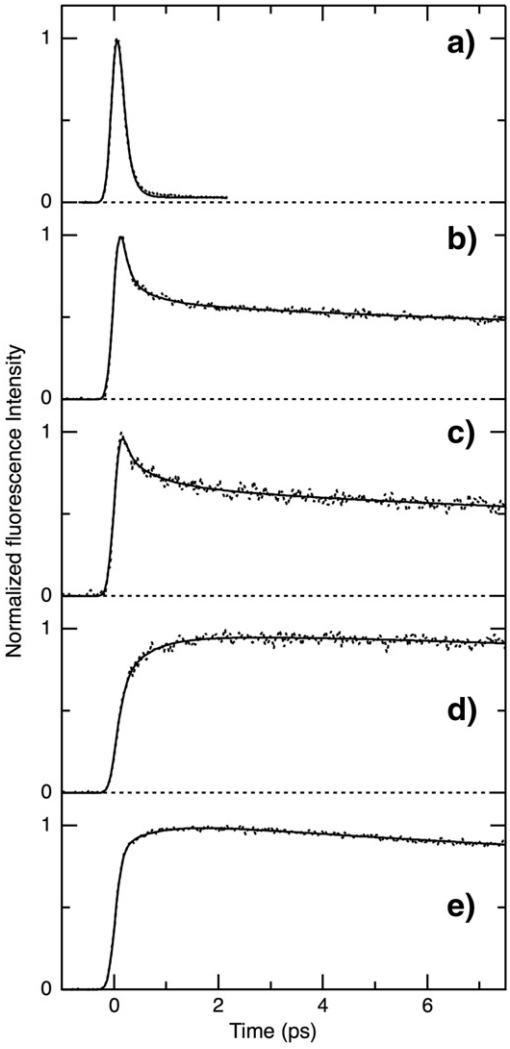

Fig. 7. Fluorescence rise and decay curves of FCPII complex: (a) 560 nm, (b) 640 nm, (c) 655 nm, (d) 677 nm, and (e) 690 nm. Dotted lines and solid lines show observed fluorescence rise and decay curves and best-fit functions, respectively. Excitation wavelength was 425 nm.

examine fluorescence kinetics more precisely, we observed fluorescence rise and decay curves with high fluorescence intensities at selected wavelengths (Fig. 7). Fluorescence rise and decay curves were analyzed by multi-exponential functions with three lifetime components in the Car fluorescence region (560 nm), and four components in the Chl fluorescence region (640 nm, 655 nm, 677 nm, and 690 nm). In these procedures, lifetime values were not globally analyzed (Eq. (3)), but freely analyzed. Table 2 summarizes the analyzed lifetime values and their amplitudes. At 560 nm, the analyzed lifetimes were the same as those obtained in the global analysis (Fig. 3). However, at 640 nm, 655 nm, 677 nm, and 690 nm, the lifetimes of the shortest-lived components were around 100 fs. These lifetime components showed positive amplitudes at 640 nm and 655 nm, and negative amplitudes at 677 nm and 690 nm. In another study, a rise time of 120 fs was resolved for Chl *a* Qy fluorescence in the *A. thaliana* LHCII [3]. Therefore, the shortest-lived components were assigned to relaxation within pigments; that is, the Qx to Qy internal conversion in Chl *a*. The decay components of 100-fs to 110-fs were a result of the short-lived Chl *a* Qx fluorescence, and possibly represented the tail of the Fx fluorescence with a 130-fs lifetime. The second lifetime components in the Chl fluorescence region were the 500-fs to 700-fs lifetime components. These components were resolved as decay components in the Chl *c* fluorescence region, and rise components in the Chl *a* fluorescence region. Therefore, we assigned this component to Chl *c*-to-Chl *a* energy transfer. In this energy transfer process, longer wavelength-form Chls (655 nm for Chl *c* and 690 nm for Chl *a*) contributed to slower energy transfer. The third lifetime components in the Chl fluorescence region were resolved as decay components in the Chl *c* fluorescence region and a rise component at 677 nm. This indicated slow-phase energy transfer between Chl *c* and Chl *a*; this transfer from Chl *c* to higher-energy Chl *a* occurred on a picosecond scale. An energy transfer pathway with time constants of a few picoseconds was resolved also in Chl *b*-to-Chl *a* energy transfer [34]. A picosecond decay component was also observed at 690 nm. This may have reflected up-hill energy transfer from lower-energy Chl *a* to higher-energy Chl *a*, which would achieve energy equilibrium among the Chls. In the Chl fluorescence region, an even longer lifetime component (>20 ps) represented energy equilibrium among Chls. The picosecond TRFS observed at 77 K are shown in Fig. S2. Just after laser excitation, Chl *a* exhibited a peak at 677 nm, but this peak shifted to 688 nm over time. The TRFS were resolved into five energy forms of Chls: one for Chl *c* and four for Chl *a* [26]. Together,

Table 1
Possible assignments for FDAS analyzed for the FCPII complex.

Time constant	Assignment
80 fs	Relaxation within Chl *c*
	Relaxation within Fx
130 fs	Relaxation within Fx
220 fs	Relaxation within Chl *a*
	Chl *c*-to-Chl *a* energy transfer
	Energy flow to lower energy form of Chl *a*
920 fs	Chl *c*-to-Chl *a* energy transfer
	Equilibration of excitation energy among Chl *a*
>1 ps	Relaxation within Fx
>10 ps	Fluorescence from the lowest excited states of Chl *c* and Chl *a*

Table 2
Analyzed fluorescence lifetimes (τ_i) and amplitudes (A_i) of fluorescence rise and decay curves of FCPII complexes isolated from *Chaetoceros gracilis*. Excitation wavelength was 425 nm. Positive and negative amplitudes indicate decay and rise components, respectively.

Wavelength (nm)	τ_1 (A_1)	τ_2 (A_2)	τ_3 (A_3)	τ_4 (A_4)
560	80 fs (0.219)	130 fs (0.769)	>1 ps (0.012)	–
640	100 fs (0.569)	510 fs (0.118)	6.1 ps (0.033)	>20 ps (0.280)
655	110 fs (0.374)	620 fs (0.155)	4.7 ps (0.059)	>20 ps (0.412)
677	100 fs (−0.458)	500 fs (−0.324)	4.4 ps (−0.121)	>20 ps (1.000)
690	90 fs (−0.310)	710 fs (−0.198)	3.2 ps (0.047)	>20 ps (0.953)

these results confirmed that Chl *a* exhibits different energy forms in the FCPII complex.

3.5. Fluorescence anisotropy decay curves of the FCPII complex

Fluorescence anisotropy decays at 677 nm and 690 nm observed using the femtosecond fluorescence up-conversion method are shown in Fig. 8. The time evolution of anisotropy depended on the wavelength; at 677 nm, the anisotropy value was less than 0.12 and independent of time, whereas at 690 nm, the initial anisotropy value was greater than 0.12 and the anisotropy decayed over time. It was reported that the anisotropy of Chl *a* Q_y fluorescence after excitation at the Soret band is 0.12 (Fig. S3a) [35]. Therefore, the anisotropy value greater than 0.12 could not be explained by relaxation within Chl *a*. In Cars, the anisotropy value of the lowest excited state is greater after excitation to the highly excited state (Fig. S3b) [28]. Therefore, the anisotropy value greater than 0.12 for the Chl *a* Qy fluorescence should reflect the energy transfer from Fx to the Chl *a* Qy band (Fig. S3c). Because higher anisotropy was observed only in the longer wavelength region, it can be concluded that lower-energy Chl *a*, such as Chl *a* exhibiting a fluorescence peak at 688 nm, received energy from Fx. This energy transfer might contribute to the red-shifted Chl *a* peak in the 220-fs FDAS (Fig. 5). The anisotropy showed decays of 300 fs (44%) and 5.2 ps (56%), which could be assigned to time constants of Fx-to-Chl *a* energy transfer and energy migration among Chl *a*, respectively [4].

4. Discussion

The picosecond TRFS of the FCPII complex suggested that the FCPII complex forms only a light-harvesting state [26]. The TRFS were globally analyzed with four time constants, 150 ps, 800 ps, 2.9 ns, and 5.6 ns; Chl *c* contributed to the former two constants, whereas Chl *a*, to all. It was found that contribution of free Chl *c* is negligibly small in the FCPII complex [26]. In the present study, we analyzed time constants of relaxation dynamics in the FCPII complex. Fx exhibited two decay lifetimes of 80 fs and 130 fs with a faint decay component (>1 ps). In terms of energy dissipation within Chls, the lifetime of the Chl *c* Soret band was 80 fs, and the time constant of the Chl *a* Qx–Qy internal conversion was determined to be ~100 fs. Energy transfer from Chl *c* to lower-energy Chl *a* occurred in 600–700 fs, whereas the energy transfer from Chl *c* to higher-energy Chl *a* had two phases; fast transfer, which occurred in 500 fs, and slow transfer, which occurred on a picosecond scale. Energy equilibrium among Chl *a* was achieved in 4 ps. The fluorescence anisotropy decayed with time constants of 300 fs and 5.2 ps, which were assigned due to Fx-to-Chl *a* energy transfer and energy migration among Chl *a*, respectively.

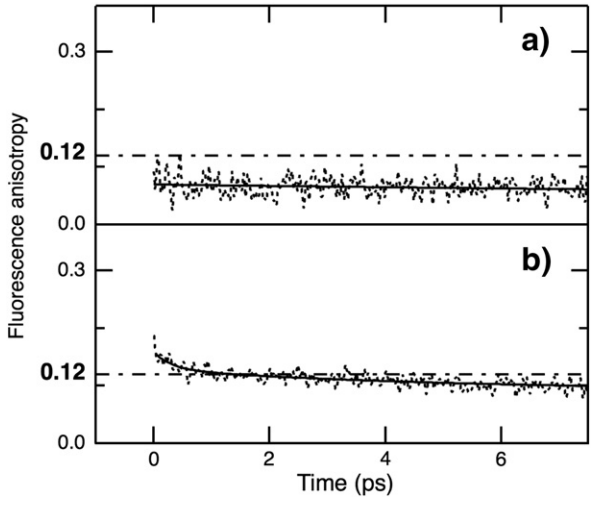

Fig. 8. Fluorescence anisotropies of FCPII complex as a function of time: (a) 677 nm and (b) 690 nm. Dotted lines and solid lines show observed fluorescence anisotropies and best-fit functions, respectively. Excitation wavelength was 425 nm. Dotted and dashed lines indicate anisotropy value of 0.12.

Previous studies on Siph in the pigment–protein complex reported that even after excitation to the S_2 state, S_2 fluorescence was not detectable because of ultrafast internal conversion, and that fluorescence from the intermediate state (S_{kc}) between the S_2 and S_1 states was observed around 580 nm [14]. In the present study, two time constants were resolved for the Fx FDAS in the FCPII complex (Fig. 5), as resolved for those in solution (Fig. 3). However, the relative amplitudes of the two FDAS differed. In solution, the amplitude of the first FDAS was five times larger than that of the second FDAS (Fig. 3), whereas, in the FCPII complex, the amplitudes of the first and second FDAS were comparable (Fig. 5). In the FCPII complex, there were two energy forms of Fxs; higher-energy Fx and lower-energy Fx, which showed prominent absorption peaks at 498 nm and 533 nm, respectively [26]. In the excitation spectrum monitored by Chl *a* fluorescence, the lower-energy Fx appeared, whereas the higher-energy Fx was absent (Fig. S4), indicating that the lower-energy Fx largely contributed to the energy transfer to Chl *a*, while the higher-energy Fx hardly contributed. This behavior was also observed in the Fx–Chl c_2-protein complex from the diatom *Cyclotella meneghiniana* [36–38]. These results indicated that the two FDAS (80 fs and 130 fs) in the FCPII complex originated from the two different energy forms of Fx. By considering the peak wavelengths, the 80-fs FDAS (peak around 580 nm) and the 130-fs FDAS (peak at 550 nm) could be assigned to the 533-nm absorption band (the lower-energy Fx) and the 498-nm absorption band (the higher-energy Fx), respectively. The observed fluorescences (the 550-nm and 580-nm bands) might originate from the S_{kc} state after the ultrafast internal conversion from the S_2 state to the S_{kc} state, as observed for Siph in the pigment–protein complex [14]. The fluorescence peak wavelength of the lower-energy Fx was the same as that of Siph in the pigment–protein complex. In this sense, the lower-energy Fx is the main keto-Car for harvesting green light, whereas the higher-energy Fx is a Car unique to the FCPII complex.

The S_{kc} lifetimes for the two energy forms of Fx were 80 fs (lower-energy Fx) and 130 fs (higher-energy). However, it is difficult to evaluate the efficiency of energy transfer from Fx(S_{kc}) to Chl accurately. Since the strength of the S_{kc}–S_0 transition in the FCPII complex was dramatically different from that in solution, we could not apply the standard method to estimate the internal conversion rate within Car in the FCPII complex [39]. The lower-energy Fx transferred energy to Chl, whereas the higher-energy Fx did not [26]. If we assume that the S_{kc} lifetime of the higher-energy Fx (130 fs) is determined only by the S_{kc}–S_1 internal conversion, then the efficiency of the Fx(S_{kc})-to-Chl energy transfer for the lower-energy Fx (80 fs) might be 38%. Since the S_{kc}

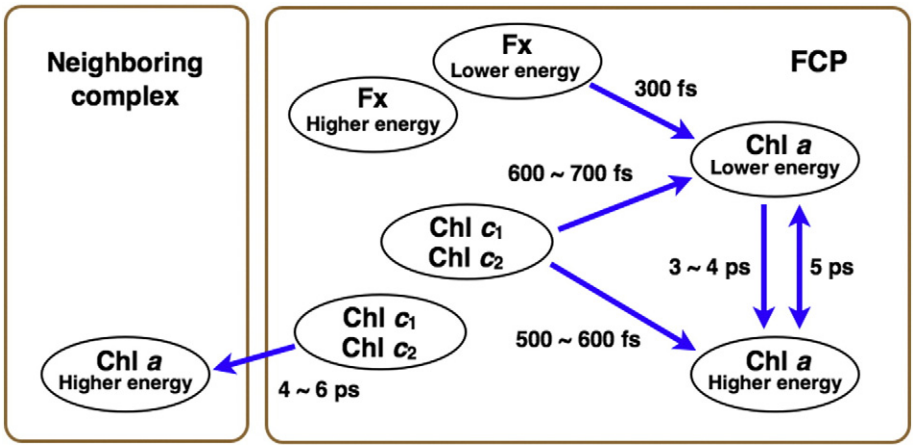

Fig. 9. Energy-transfer pathways and their time constants revealed by the present study; 5-ps component represents energy migration among Chl.

state of the lower-energy Fx is located at 1300 cm^{-1} lower energy than that of the higher-energy Fx, it is expected that rate constant of the S_{kc}–S_1 internal conversion is larger than (130 fs)$^{-1}$ based on the energy gap law [39,40]. Therefore, the efficiency of the Fx(S_{kc})-to-Chl energy transfer was estimated to be less than 38%. This value is not enough to explain efficient energy transfer from Fx to Chl *a* [30], indicating that the energy transfer pathway from the S_1 state should be dominant. Through the fluorescence anisotropy decay at 690 nm, the time constant for Fx-to-Chl *a* energy transfer was estimated to be 300 fs. Based on the S_1 lifetime value of Fx in solution (41 ps) [41], the efficiency of the Fx(S_1)-to-Chl *a* energy transfer was evaluated as almost unity, as was obtained for other keto-Cars, Siph [4] and peridinin [42].

For the Chl *c*-to-Chl *a* energy transfer, the time constants were determined to be 500 fs, 600–700 fs, and 4.7–6.1 ps (Table 2). The time constants of 500–700 fs are comparable to those determined for Chl *b*-to-Chl *a* energy transfer [3]. Although the time constants of 4.7–6.1 ps are somewhat longer, the efficiency of the Chl *c*-to-Chl *a* energy transfer was calculated to be almost unity because of the long S_1 lifetime of Chl *c* (~4 ns, unpublished data). Energy was transferred very efficiently from Chl *c* to Chl *a*; however, a peak for Chl *c* was clearly observed in the steady-state fluorescence spectrum (Fig. 1). This was also observed in the spectrum of the FCP complex isolated from the brown alga *Dictyota dichotoma* [13,30]. These results indicated that some Chl *c* retained excitation energy in the isolated FCPII complex in the time region examined here. In the later time region, Chl *c* exhibited decays of 150 ps and 800 ps in the isolated FCPII complex [26]. Therefore, the contribution of Chl *c* to the steady-state fluorescence spectrum around 640 nm could be ascribed to the 150-ps and 800-ps components. To precisely examine the slow-phase Chl *c*-to-Chl *a* energy transfer, we measured fluorescence rise and decay curves of the *C. gracilis* cells (Fig. S5). There were large differences in the third and longest-lived decay components of Chl *c* fluorescences between the isolated FCPII complexes and the intact cells. The contributions of the third components were larger and those of the longest-lived components were smaller in the intact cells than in the isolated complexes (Table S1). The amplitudes of the third components in the cells were 4.6 to 7.2 times larger than those in the complexes, which could not be explained by relaxation within Chl *c*. Therefore, we assigned the third components in the cells to the slow-phase Chl *c*-to-Chl *a* energy transfer as is the case for the FCPII complexes. The contribution of the corresponding rise component (the third component at 677 nm) did not become larger in the cells. This is probably because relative amount of Chl *a* is larger in the cells due to the existence of PSI and PSII core complexes. The contribution of the slow-phase Chl *c*-to-Chl *a* energy was much larger in the cells, indicating that the slow-phase Chl *c*-to-Chl *a* energy transfer could be assigned to inter-complex energy transfer. This assignment was confirmed by the steady-state fluorescence measurements, since the Chl *c* fluorescence peak was absent from the spectra of *C. gracilis* cells (Fig. S1). It is likely that some Chl *c* does not transfer energy to Chl *a* within the FCPII complex in the time region examined here, and that for this type of Chl *c*, inter-complex energy transfer pathways are established instead of intra-complex pathways.

5. Summary

The excitation-relaxation and energy-transfer processes in the FCPII complex from *C. gracilis* revealed by the present study are summarized in Fig. 9. Lower-energy Fx transferred excitation energy to lower-energy Chl *a* with a time constant of 300 fs. Chl *c* transferred excitation energy to (1) higher-energy Chl *a* with a time constant of 500–600 fs (intra-complex), (2) lower-energy Chl *a* with a time constant of 600–700 fs (intra-complex), and (3) higher-energy Chl *a* with a time constant of 4–6 ps (inter-complex). The first and second processes were comparable to the Chl *b* to Chl *a* energy transfer in the LHCII from the green alga *C. fragile* and the higher plant *A. thaliana*. In *C. gracilis* cells, the third process made a greater contribution to the total Chl *c*-to-Chl *a* transfer than did the first and second processes. Chl *a* exhibited different energy forms with fluorescence peaks ranging from 677 nm to 688 nm. The lower-energy Chl *a* worked as a relay pigment in energy transfer; it received excitation energy from Fx and transferred the energy to higher-energy Chl *a*.

Supplementary data to this article can be found online at http://dx.doi.org/10.1016/j.bbabio.2014.02.002.

Acknowledgements

This work was supported by Grant-in-Aids for Scientific Research from the Ministry of Education of Japan (22370017 to T.T. and S.A. and 21570038 to T.T.), a Grant-in-Aid for JSPS Fellows no. 21-2944 (M.Y.), a grant from JST PRESTO (T.T.), and a grant from the Australian Research Council's Discovery Projects funding scheme (project number DP12101360) to T.T.

References

[1] B.R. Green, J.M. Anderson, W.W. Parson, Photosynthetic membranes and their light-harvesting antennas, in: B.R. Green, W.W. Parson (Eds.), Light-harvesting Antennas in Photosynthesis, Kluwer Academic Publishers, Dordrecht, The Netherlands, 2003, pp. 1–28.
[2] W. Rüdiger, S. Schoch, Chlorophylls, in: T.W. Goodwin (Ed.), Plant Pigments, Academic Press Ltd., London, UK, 1988, pp. 1–59.
[3] S. Akimoto, M. Yokono, M. Ohmae, I. Yamazaki, A. Tanaka, M. Higuchi, T. Tsuchiya, H. Miyashita, M. Mimuro, Ultrafast excitation relaxation dynamics of lutein in solution and in the light-harvesting complexes II isolated from *Arabidopsis thaliana*, J. Phys. Chem. B 109 (2005) 12612–12619.

[4] S. Akimoto, I. Yamazaki, A. Murakami, S. Takaichi, M. Mimuro, Ultrafast excitation relaxation dynamics and energy transfer in the siphonaxanthin-containing green alga *Codium fragile*, Chem. Phys. Lett. 390 (2004) 45–49.
[5] T. Förster, Intermolecular energy migration and fluorescence, Ann. Phys. 2 (1948) 55–75.
[6] A.J. Young, Occurrence and distribution of carotenoids in photosynthetic systems, in: A. Young, G. Britton (Eds.), Carotenoids in Photosynthesis, Chapman & Hall, London, UK, 1993, pp. 16–71.
[7] Y. Koyama, M. Kuki, P.O. Andersson, T. Gillbro, Singlet excited states and the light-harvesting function of carotenoids in bacterial photosynthesis, Photochem. Photobiol. 63 (1996) 243–256.
[8] H.A. Frank, R.J. Cogdell, Carotenoids in photosynthesis, Photochem. Photobiol. 63 (1996) 257–264.
[9] R.G. Hiller, Carotenoids as components of light-harvesting proteins of eukaryotic algae, in: H.A. Frank, A.J. Young, G. Britton, R.J. Cogdell (Eds.), The Photochemistry of Carotenoids, Kluwer Academic Publishers, Dordrecht, Netherland, 1999, pp. 81–98.
[10] W. Kühlbrandt, D.N. Wang, Y. Fujiyoshi, Atomic model of plant light-harvesting complex by electron crystallography, Nature 367 (1994) 614–621.
[11] E.J.G. Peterman, R. Monshouwer, I.H.M. van Stokkum, R. van Grondelle, H. van Amerongen, Ultrafast singlet excitation transfer from carotenoids to chlorophylls via different pathways in light-harvesting complex II of higher plants, 264 (1997) 279–284.
[12] R. Croce, S. Weiss, R. Bassi, Carotenoid-binding sites of the major light-harvesting complex II of higher plants, J. Biol. Chem. 274 (1999) 29613–29623.
[13] T. Katoh, M. Mimuro, S. Takaichi, Light-harvesting particles isolated from a brown alga, *Dictyota dichotoma*. A supramolecular assembly of fucoxanthin–chlorophyll-protein complexes, Biochim. Biophys. Acta 976 (1989) 233–240.
[14] S. Akimoto, T. Tomo, Y. Naitoh, A. Otomo, A. Murakami, M. Mimuro, Identification of a new excited state responsible for the in vivo unique absorption band of siphonaxanthin in the green alga *Codium fragile*, J. Phys. Chem. B 111 (2007) 9179–9181.
[15] W. Wang, X. Qin, M. Sang, D. Chen, K. Wang, R. Lin, C. Lu, J.-R. Shen, T. Kuang, Spectral and functional studies on siphonaxanthin-type light-harvesting complex of photosystem II from *Bryopsis corticulans*, Photosynth. Res. 117 (2013) 267–279.
[16] C.B. Field, M.J. Behrenfeld, J.T. Randerson, P. Falkowski, Primary production of the biosphere: integrating terrestrial and oceanic components, Science 281 (1998) 237–240.
[17] L.K. Medlin, I. Kaczmarska, Evolution of diatoms. V. Morphological and cytological support for the major clades and a taxonomic revision, Phycologia 43 (2004) 245–270.
[18] C. Büchel, Fucoxanthin–chlorophyll proteins in diatoms: 18 and 19 kDa subunits assemble into different oligomeric states, Biochemistry 42 (2003) 13027–13034.
[19] T. Brakemann, W. Schlörmann, J. Marquardt, M. Nolte, E. Rhiel, Association of fucoxanthin chlorophyll *a*/*c*-binding polypeptides with photosystems and phosphorylation in the centric diatom *Cyclotella cryptica*, Protist 157 (2006) 463–475.
[20] B. Lepetit, D. Volke, M. Szabó, R. Hoffmann, G. Garab, C. Wilhelm, R. Goss, Spectroscopic and molecular characterization of the oligomeric antenna of the diatom *Phaeodactylum tricornutum*, Biochemistry 46 (2007) 9813–9822.
[21] I. Grouneva, A. Rokka, E.-M. Aro, The thylakoid membrane proteome of two marine diatoms outlines both diatom-specific and species-specific features of the photosynthetic machinery, J. Proteome Res. 10 (2011) 5338–5353.
[22] R. Nagao, T. Tomo, E. Noguchi, T. Suzuki, A. Okumura, R. Narikawa, I. Enami, M. Ikeuchi, Proteases are associated with a minor fucoxanthin chlorophyll *a*/*c*-binding protein from the diatom, *Chaetoceros gracilis*, Biochim. Biophys. Acta 1817 (2012) 2110–2117.
[23] R. Nagao, M. Yokono, S. Akimoto, T. Tomo, High excitation energy quenching in fucoxanthin chlorophyll *a*/*c*-binding protein complexes from the diatom *Chaetoceros gracilis*, J. Phys. Chem. B 117 (2013) 6888–6895.
[24] R. Nagao, S. Takahashi, T. Suzuki, N. Dohmae, K. Nakazato, T. Tomo, Comparison of oligomeric states and polypeptide compositions of fucoxanthin chlorophyll *a*/*c*-binding protein complexes among various diatom species, Photosynth. Res. 117 (2013) 281–288.
[25] R. Nagao, A. Ishii, O. Tada, T. Suzuki, N. Dohmae, A. Okumura, M. Iwai, T. Takahashi, Y. Kashino, I. Enami, Isolation and characterization of oxygen-evolving thylakoid membranes and photosystem II particles from a marine diatom *Chaetoceros gracilis*, Biochim. Biophys. Acta 1767 (2007) 1353–1362.
[26] R. Nagao, M. Yokono, A. Teshigahara, S. Akimoto, T. Tomo, Light-harvesting ability of the fucoxanthin chlorophyll a/c-binding protein associated with photosystem II from the diatom Chaetoceros gracilis as revealed by picosecond time-resolved fluorescence spectroscopy (submitted for publication).
[27] R. Nagao, T. Tomo, E. Noguchi, S. Nakajima, T. Suzuki, A. Okumura, Y. Kashino, M. Mimuro, M. Ikeuchi, I. Enami, Purification and characterization of a stable oxygen-evolving photosystem II complex from a marine centric diatom, *Chaetoceros gracilis*, Biochim. Biophys. Acta 1797 (2010) 160–166.
[28] S. Akimoto, M. Mimuro, Application of time-resolved polarization fluorescence spectroscopy in the femtosecond range to photosynthetic systems, Photochem. Photobiol. 83 (2007) 163–170.
[29] S. Akimoto, M. Yokono, F. Hamada, A. Teshigahara, S. Aikawa, A. Kondo, Adaptation of light-harvesting systems of *Arthrospira platensis* to light conditions, probed by time-resolved fluorescence spectroscopy, Biochim. Biophys. Acta 1817 (2012) 1483–1489.
[30] M. Mimuro, T. Katoh, H. Kawai, Spatial arrangement of pigments and their interactions in the fucoxanthin–chlorophyll *a*/*c* protein assembly (FCPA) isolated from the brown alga *Dictyota dichotoma*. Analysis by means of polarized spectroscopy, Biochim. Biophys. Acta 1015 (1990) 450–456.
[31] S. Akimoto, T. Yamazaki, I. Yamazaki, A. Osuka, Excitation relaxation of zinc and free-base porphyrin probed by femtosecond fluorescence spectroscopy, Chem. Phys. Lett. 309 (1999) 177–182.
[32] S. Akimoto, M. Yokono, M. Higuchi, T. Tomo, S. Takaichi, A. Murakami, M. Mimuro, Solvent effects on excitation relaxation dynamics of a keto-carotenoid, siphonaxanthin, Photochem. Photobiol. Sci. 7 (2008) 1206–1209.
[33] D. Kosumi, T. Kusumoto, R. Fujii, M. Sugisaki, Y. Iinuma, N. Oka, Y. Takaesu, T. Taira, M. Iha, H.A. Frank, H. Hashimoto, Ultrafast excited state dynamics of fucoxanthin: excitation energy dependent intramolecular charge transfer dynamics, Phys. Chem. Chem. Phys. 13 (2011) 10762–10770.
[34] J.P. Connelly, M.G. Müller, R. Bassi, R. Croce, A.R. Holzwarth, Femtosecond transient absorption study of carotenoid to chlorophyll energy transfer in the light-harvesting complex II of photosystem II, Biochemistry 36 (1997) 281–287.
[35] M. van Grup, G. van Ginkel, Y.K. Levine, Fluorescence anisotropy of chlorophyll *a* and chlorophyll *b* in castor oil, Biochim. Biophys. Acta 973 (1989) 405–413.
[36] E. Papagiannakis, I.H.M. van Stokkum, H. Fey, C. Büchel, R. van Grondelle, Spectroscopic characterization of the excitation energy transfer in the fucoxanthin–chlorophyll protein of diatoms, Photosynth. Res. 86 (2005) 241–250.
[37] L. Premvardhan, D.J. Sandberg, H. Fey, R.R. Birge, C. Büchel, R. van Grondelle, The charge-transfer properties of the S_2 state of fucoxanthin in solution and in fucoxanthin chlorophyll-a/c_2 protein (FCP) based on stark spectroscopy and molecular-orbital theory, J. Phys. Chem. B 112 (2008) 11838–11853.
[38] N. Gildenhoff, S. Amarie, K. Gundermann, A. Beer, C. Büchel, J. Wachtveitl, Oligomerization and pigmentation dependent excitation energy transfer in fucoxanthin–chlorophyll proteins, Biochim. Biophys. Acta 1797 (2010) 543–549.
[39] M. Ricci, S.E. Bradforth, R. Jimenez, G.R. Fleming, Internal conversion and energy transfer dynamics of shperoidene in solution and in the LH-1 and LH-2 light-harvesting complexes, Chem. Phys. Lett. 259 (1996) 381–390.
[40] R. Englman, J. Jortner, The energy gap law for radiationless transitions in large molecules, Mol. Phys. 18 (1970) 145–164.
[41] T. Katoh, U. Nagashima, M. Mimuro, Fluorescence properties of the allenic carotenoid fucoxanthin: implication for energy transfer in photosynthetic pigment systems, Photosynth. Res. 27 (1991) 221–226.
[42] T. Polívka, I.H.M. Stokkum, D. Zigmantas, R. van Grondelle, V. Sundström, R.G. Hiller, Energy transfer in the major intrinsic light-harvesting complex from *Amphidinium carterae*, Biochemistry 45 (2006) 8516–8526.